 CMC, vol.23, no.1, pp.9-34, 2011

A Coupling Algorithm of Finite Element Method and Smoothed Particle Hydrodynamics for Impact Computations

Yihua Xiao[1], **Xu Han**[1,2] **and Dean Hu**[1]

Abstract: For impact computations, it is efficient to model small and large deformation regions by Finite Element Method (FEM) and Smoothed Particle Hydrodynamics (SPH), respectively. However, it requires an effective algorithm to couple FEM and SPH calculations. To fulfill this requirement, an alternative coupling algorithm is presented in this paper. In the algorithm, the coupling between element and particle regions are achieved by treating elements as imaginary particles and applying equivalent tractions to element sides on coupling interfaces. In addition, an adaptive coupling technique is proposed based on the algorithm to improve the computational efficiency of FEM-SPH coupling further. For this technique, the initial model can totally consist of elements. During the deformation process distorted elements are converted to particles automatically and the generated particles are linked to adjacent elements with the present coupling algorithm. Several examples are included to demonstrate the accuracy and utility of the present coupling algorithm and adaptive coupling technique.

Keywords: impact; coupling algorithm; adaptive coupling; FEM; SPH

1 Introduction

Impact problems exist in many fields of engineering. They often involve severe deformations of materials. To simulate this kind of problems, Finite Element Method (FEM) suffers from mesh tangling. Though element erosion and remeshing techniques can be used to overcome the problem in some extent, the former leads to some artificial effects and the later increases the computational cost significantly. Smoothed particle hydrodynamics (SPH) [Lucy (1977); Gingold and Monaghan (1977)] as a meshless, lagrangian particle method is good at treating large defor-

[1] State Key Laboratory of Advanced Design and Manufacturing for Vehicle Body, Hunan University, Changsha, China, 410082

[2] Corresponding author: hanxu@hnu.edu.cn; Fax: +86 0731 88822051

mations. It is suited for impact simulation. But SPH is more computationally expensive than FEM. To develop a good method for impact simulation, coupling of FEM and SPH seems an effective approach. Since for most impact problems large deformations focus on limited impact regions and most regions deform slightly, so one can use SPH only in impact regions to capture large deformations and FEM in most regions to speed up the computation. Then, good computational accuracy and efficiency can be obtained simultaneously.

In order to couple FEM and SPH, it is necessary to resolve two essential problems. One is the contact of particles and elements from different bodies, and the other is the coupling of particles and elements in the same bodies. The particle-element contact is relatively easy to treat since some well-developed contact algorithms in FEM can be used as the basis and little modifications should be made. Now, several effective particle-element contact algorithms are available for engineering applications [Attaway, Heinstein and Swegle (1994); Johnson, Stryk and Beissel (1996a); De Vuyst, Vignjevic and Campbell (2005)]. The particle-element coupling is hard to handle, because there are large differences between FEM and SPH in the variable interpolation and discretization of governing equations. In this paper, we attempt to develop an accurate and efficient algorithm for the particle-element coupling.

Some algorithms have been proposed to treat the particle-element coupling now. Johnson et al. [Johnson (1994)] proposed an algorithm which fixes particles to element nodes. The algorithm is very simple in implementation, but its drawbacks are that stress oscillation exists [Johnson, Stryk and Beissel (1996b)] and the particle arrangement is limitary near coupling interfaces. Fernández-Méndez et al. [Fernández-Méndez, Bonet and Huerta (2005)] developed an algorithm for the continuous blending of FEM and SPH. This algorithm ensures the continuity of the interpolation in the global problem domain, but it requires transition regions. Sauer [Sauer (2000)] suggested a hybrid coupling algorithm, which includes the effects of elements in the SPH approximation by Gauss quadrature. He also proposed an adaptive coupling approach based on the hybrid algorithm [Sauer (2000)] and applied it to model penetration events [Sauer, Hiermeier, and Scheffer (2001)]. Besides the above-mentioned algorithms, there are still other algorithms for coupling particles with elements, such as the master-slave coupling in Rabczuk, Xiao and Sauer (2006) and matching algorithm in Johnson, Stryk, Beissel and Holmquist (2002) and Johnson and Stryk (2003). These algorithms are not specially developed for SPH, but they have general applicability for particle methods and can be directly applied to SPH.

In this paper, we present an alternative algorithm for particle-element coupling. The algorithm treats elements near coupling interfaces as imaginary particles to

calculate forces on particles from adjacent elements. It imposes equivalent tractions to element sides on coupling interfaces according to the stresses of particles associated to them for calculating forces on element nodes from adjacent particles. The algorithm is simple in implementation and produces better coupling accuracy than some existing coupling algorithms. It needs no transition region. Based on this algorithm, an adaptive coupling technique is also proposed.

The rest of the paper is organized as follows. Section 2 introduced the basic equations of SPH used in this paper briefly. Section 3 details the present coupling algorithm. Section 4 describes the adaptive coupling technique. Section 5 presents several numerical examples to validate the coupling algorithm and adaptive coupling technique. The final section draws conclusions of the present work.

2 Basic equations of SPH

The SPH equations used in this paper are given as follows

$$\dot{\rho}_i = \sum_{j=1}^{N} m_j (v_i^\beta - v_j^\beta) \frac{\partial W_{ij}}{\partial x_i^\beta} \tag{1}$$

$$\frac{dv_i^\alpha}{dt} = \sum_{j=1}^{N} m_j \left(\frac{\sigma_i^{\alpha\beta}}{\rho_i^2} + \frac{\sigma_j^{\alpha\beta}}{\rho_j^2} + \Pi_{ij}\delta^{\alpha\beta} \right) \frac{\partial W_{ij}}{\partial x_i^\beta} \tag{2}$$

$$\frac{de_i}{dt} = \frac{1}{2} \sum_{j=1}^{N} m_j \left(\frac{\sigma_i^{\alpha\beta}}{\rho_i^2} + \frac{\sigma_j^{\alpha\beta}}{\rho_j^2} + \Pi_{ij}\delta^{\alpha\beta} \right) \left(v_j^\alpha - v_i^\alpha \right) \frac{\partial W_{ij}}{\partial x_i^\beta} \tag{3}$$

where ρ is the density, m is the mass, v is the velocity, σ is the stress, e is the specific internal energy per unit mass, x is the coordinate, i and j are particle indices, W is the kernel function, and Π is the artificial viscosity. It is referred to [Liu and Liu (2003)] for detailed derivation of Equation (1)-(3).

For the kernel function W, the B-spline function is used, which is defined as

$$W_{ij} = W\left(d_{ij}, \bar{h}_{ij}\right) = \alpha_d \times \begin{cases} 2/3 - \xi^2 + \xi^3/2, & 0 \le \xi < 1 \\ (2-\xi)^3/6, & 1 \le < 2 \\ 0, & \xi \ge 2 \end{cases} \tag{4}$$

where $\xi = d_{ij}/\bar{h}_{ij}$, $d_{ij} = \sqrt{x_{ij}^\alpha x_{ij}^\alpha}$, $x_{ij}^\alpha = x_i^\alpha - x_j^\alpha$, $\bar{h}_{ij} = 0.5(h_i + h_j)$, h is the smoothing length, and α_d is a constant dependent on the problem dimension, which is taken as $15/7\pi h^2$ for two-dimensional problem. The initial smoothing length is given as

$$h_0 = \alpha_h \Delta \tag{5}$$

where h_0 is the initial smoothing length, α_h is a dilation factor and Δ is the particle spacing. The smoothing length is updated with

$$h = h_0 \left(\frac{\rho_0}{\rho} \right)^{1/2} \tag{6}$$

For the artificial viscosity Π, the expression suggested by Monaghan [Monaghan (1992)] is used, which is given as

$$\Pi_{ij} = \begin{cases} \frac{-\alpha_\Pi \bar{c}_{ij} \varphi_{ij} + \beta_\Pi \varphi_{ij}^2}{\bar{\rho}_{ij}} & v_{ij}^\alpha x_{ij}^\alpha < 0 \\ 0 & v_{ij}^\alpha x_{ij}^\alpha \geq 0 \end{cases} \tag{7}$$

where $\bar{c}_{ij} = \frac{1}{2}(c_i + c_j)$, $\varphi_{ij} = \frac{\bar{h}_{ij} v_{ij}^\alpha x_{ij}^\alpha}{|d_{ij}|^2 + \phi^2}$, $\phi = 0.1\bar{h}_{ij}$, $\bar{\rho}_{ij} = \frac{1}{2}(\rho_i + \rho_j)$, c denotes the speed of sound, and the constants, α_Π and β_Π, are both set to 1.0.

The tensile instability is an important problem of SPH. We follow the artificial stress method in Gray and Monaghan (2001) to overcome the problem.

3 Coupling algorithm of FEM and SPH

In order to couple FEM and SPH, the crucial problem is to calculate the forces exchanging between elements and particles near coupling interfaces. We present a new coupling algorithm to calculate these forces. The basic principle of the algorithm is shown in Figure 1. On the one hand, elements near coupling interfaces are treated as imaginary particles. Including these imaginary particles in SPH calculations provides the forces on particles form adjacent elements. On the other hand, equivalent tractions are determined based on adjacent particles of elements and considered to impose on element sides composing coupling interfaces. Then, distributing these tractions to element nodes gives the forces on element nodes from adjacent particles. The details of the algorithm are described in the following of this section.

3.1 Determination of elements treated as imaginary particles

Elements covered by influence domains of particles are treated as imaginary particles. A search is required to determine those elements. One may choose to perform the search at either the beginning or each cycle of the computation. Searching at the beginning requires needs search for only one time, but more elements should be included because it is necessary to contains all elements probably covered by influence domains of real particles during the whole computation. Searching at each cycle obtains the least elements, but an efficient algorithm is required to reduce the

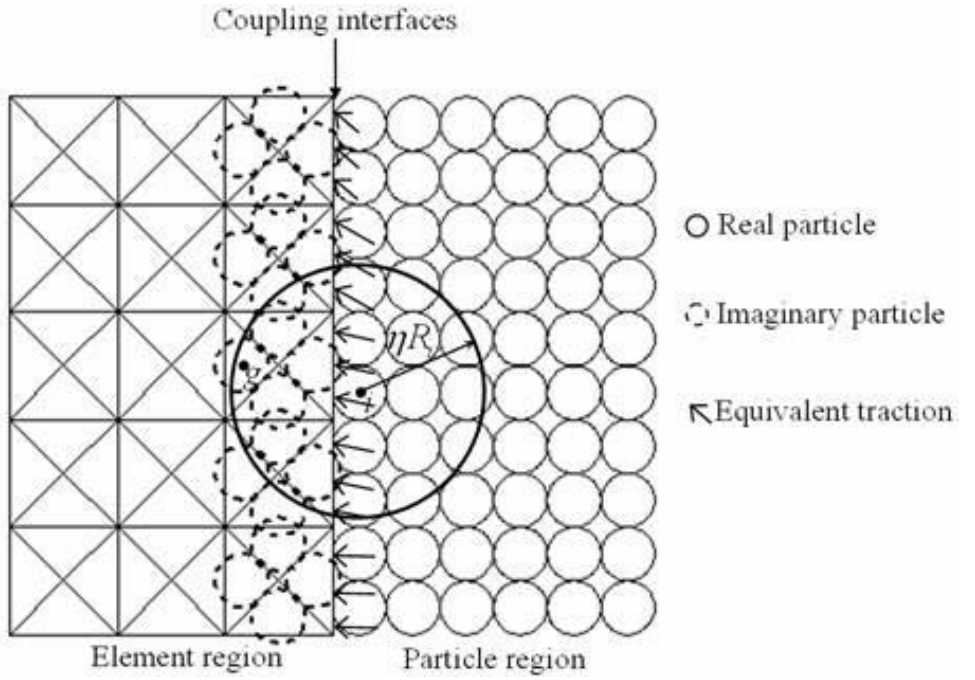

Figure 1: Basic principle for computing forces exchanging between elements and particles near coupling interfaces

computational cost of the search. Considering that deformations near coupling interfaces are generally not serious and elements treated as imaginary particles will not change dramatically in the computation process, so we here suggest a simple procedure to identify those elements at the beginning of the computation.

For an arbitrary element, we check the following condition

$$d_{gi} < \eta R_i \tag{8}$$

where d_{gi} is the distance from the gravity center of the element to the center of particle i, $R_i = 2h_i$ is the radius of the influence domain of particle i, and η is a dilation factor. If there is a particle satisfying this condition for the element, then the element is identified as one need to treat as imaginary particle.

The dilation factor η in Equation (8) is larger than 1. It is used to include the elements which are not needed to treat as imaginary particles at initial time but probably needed after deformation. Generally, $\eta = 1.5$ is large enough to make all the elements needed to treat as imaginary particles identified during the whole

computation process. Unless otherwise specified in this paper, η is always taken as that value.

3.2 Generation of imaginary particles

Imaginary particles are embedded into elements treated as imaginary particles. Theoretically, it is possible to embed multi particles in one element, but only discussed here is the simplest case which is one particle for one element. Imaginary particles should be renewedly generated in each computation cycle. The variables of them are obtained from the corresponding elements where they are embedded. Figure 2 shows an imaginary particle generated from an element. A detailed description for the determination of variables of the imaginary particle is given as follows:

(a) The mass and density are given as

$$m_{\mathrm{IP}i} = m_{\mathrm{E}I}, \quad \rho_{\mathrm{IP}i} = \rho_{\mathrm{E}I} \tag{9}$$

where "$_{\mathrm{IP}}$" and "$_{\mathrm{E}}$" denote variables of imaginary particles and elements, respectively, and the subscripts "$_i$" and "$_I$" are indices of imaginary particles and elements, respectively.

(b) The coordinates and velocities are taken as the average of those of the three element nodes

$$x^{\alpha}_{\mathrm{IP}i} = \bar{x}^{\alpha}_{\mathrm{E}I} = (x^{\alpha}_{\mathrm{E}R} + x^{\alpha}_{\mathrm{E}S} + x^{\alpha}_{\mathrm{E}T})/3 \tag{10}$$

$$v^{\alpha}_{\mathrm{IP}i} = \bar{v}^{\alpha}_{\mathrm{E}I} = (v^{\alpha}_{\mathrm{E}R} + v^{\alpha}_{\mathrm{E}S} + v^{\alpha}_{\mathrm{E}T})/3 \tag{11}$$

where R, S and T are indices of the three nodes of element I.

(c) The radius is given as

$$r_{\mathrm{IP}i} = \frac{\sqrt{A_{\mathrm{E}I}}}{2} \tag{12}$$

where $A_{\mathrm{E}I}$ is the area of element I. The smoothing length is determined as

$$h_{\mathrm{IP}i} = \alpha_h \sqrt{A_{\mathrm{E}I}} \tag{13}$$

(d) The stresses equal to those of the element

$$\sigma^{\alpha\beta}_{\mathrm{IP}i} = \sigma^{\alpha\beta}_{\mathrm{E}I} \tag{14}$$

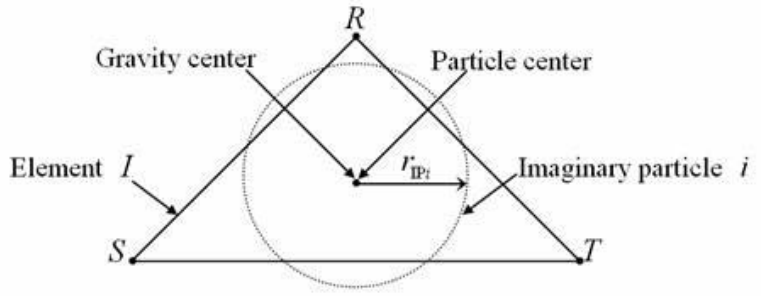

Figure 2: An imaginary particle generated from an element

3.3 Calculation of forces on particles from adjacent elements

The forces on particles near coupling interfaces come from their adjacent elements and real particles. Figure 3 shows the calculation of these forces. The influence domain of particle i contains both real particles $(n_1, \ldots n_{12})$ and imaginary particles $(n_{13}, \ldots n_{19})$. For calculating the forces on particle i, both the imaginary and real particles are included in the sums of SPH equations. When imaginary particles are added, SPH equations become

$$\dot{\rho}_i = \sum_{j=1}^{N_{\mathrm{RP}}+N_{\mathrm{IP}}} m_j (v_i^\beta - v_j^\beta) \frac{\partial W_{ij}}{\partial x_i^\beta} \tag{15}$$

$$\frac{dv_i^\alpha}{dt} = \sum_{j=1}^{N_{\mathrm{RP}}+N_{\mathrm{IP}}} m_j \left(\frac{\sigma_i^{\alpha\beta}}{\rho_i^2} + \frac{\sigma_j^{\alpha\beta}}{\rho_j^2} + \Pi_{ij}\delta^{\alpha\beta} \right) \frac{\partial W_{ij}}{\partial x_i^\beta} \tag{16}$$

$$\frac{de_i}{dt} = \frac{1}{2} \sum_{j=1}^{N_{\mathrm{R}}+N_{\mathrm{IP}}} m_j \left(\frac{\sigma_i^{\alpha\beta}}{\rho_i^2} + \frac{\sigma_j^{\alpha\beta}}{\rho_j^2} + \Pi_{ij}\delta^{\alpha\beta} \right) \left(v_j^\alpha - v_i^\alpha \right) \frac{\partial W_{ij}}{\partial x_i^\beta} \tag{17}$$

where N_{RP} and N_{IP} are the number of real and imaginary particles in the influence domain of particle i, respectively. In Equation (16), the force contributions of the imaginary particles give the forces on particle i from its adjacent elements.

In addition, the imaginary particles are also used in the calculation of strain rates. This reduces the error of SPH approximation near coupling interfaces, so strain rates and resultant stresses can be computed accurately. Figure 4(a) shows a square patch discretized with 400 real particles in the central region $([-0.5, 0.5] \times [-0.5, 0.5])$ and 1200 elements in the outer regions. The elements and particles are uniform. The patch is given velocities defined by $v^1 = v^2 = x^1 + x^2$. The strain rates $\dot{\varepsilon}^{11}$ for particles are calculated to test the effects of the imaginary particles. Figures 4(b)

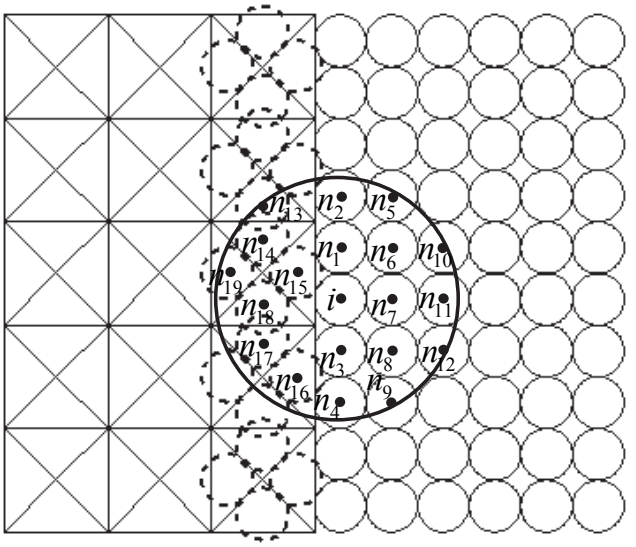

Figure 3: Calculation of forces on particles near coupling interfaces

and (c) show the strain rates in the central particle region calculated with and without imaginary particles in elements near coupling interfaces, respectively. It can be seen that the strain rates calculated with imaginary particles is much more accurate than those calculated without imaginary particles.

3.4 Calculation of forces on element nodes from adjacent particles

Figure 5 illustrates the calculation of the forces on element nodes from adjacent particles. For each element side on coupling interfaces, an equivalent traction is determined according to the stresses of its adjacent particles and considered to uniformly impose on it. The equivalent tractions are expressed as

$$t_{IJ}^{\alpha} = \bar{\sigma}^{\alpha\beta} n^{\beta} \tag{18}$$

$$\bar{\sigma}^{\alpha\beta} = \sum_{j=1}^{N_s} \sigma_j^{\alpha\beta} / N_s \tag{19}$$

where t_{IJ}^{α} is the equivalent traction, n^{β} is the unit outward normal vector of element side IJ, $\sigma_j^{\alpha\beta}$ denotes the stresses of the particles associated to element side IJ, and

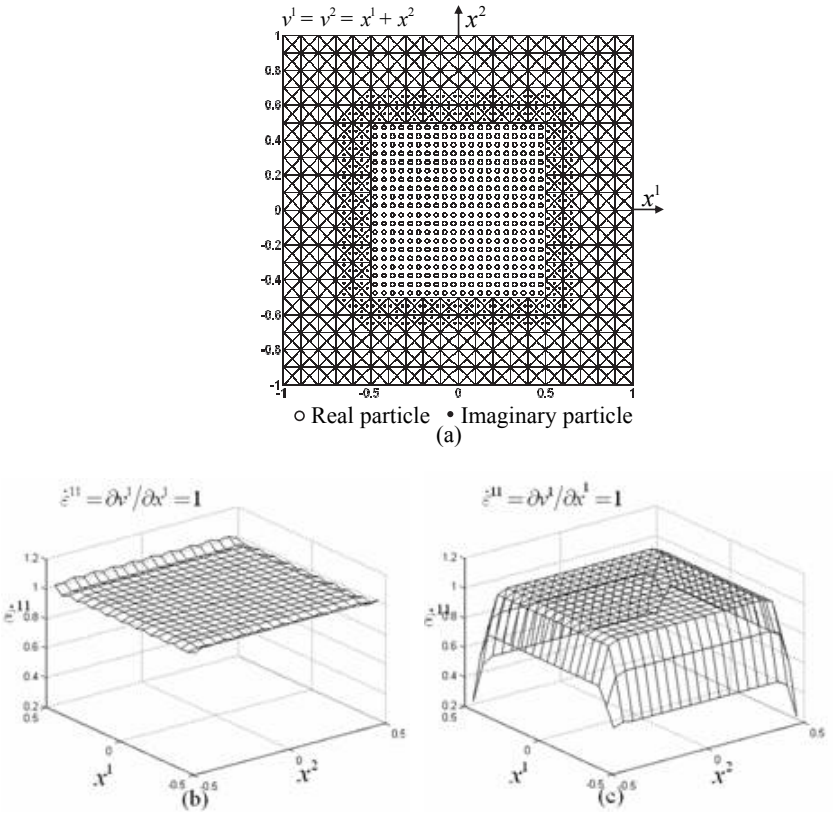

Figure 4: Strain rates in the central particle region of a square patch with a hybrid discretization of elements and particles: (a) Discretization of the patch; (b) Strain rates calculated with imaginary particle; (c) Strain rates calculated without imaginary particle

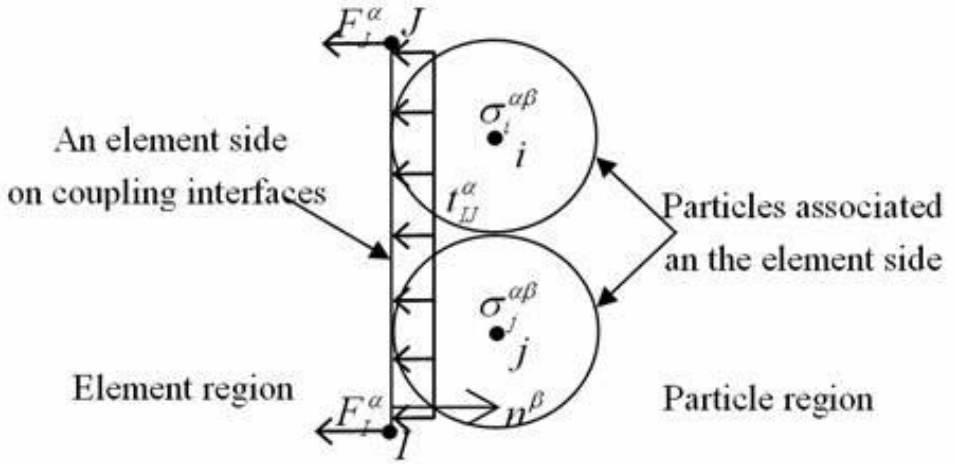

Figure 5: Calculation of forces on element nodes from adjacent particles

N_s is the number of the particles associated to element side IJ. The determination of particles associated to an element side will be described later.

After determining the equivalent traction, the total force on element side IJ can be easily calculated as

$$F_{IJ}^{\alpha} = t_{IJ}^{\alpha} lT \tag{20}$$

where l is the length of the element side, and T is the thickness of the element. In our calculation, T is assumed to be unit for 2D plane problem, so we have

$$F_{IJ}^{\alpha} = t_{IJ}^{\alpha} l \tag{21}$$

Distributing the total force to the nodes of element side IJ uniformly, the forces on element nodes from adjacent particles are finally obtained as

$$F_I^{\alpha} = F_J^{\alpha} = \frac{1}{2} F_{IJ}^{\alpha} = \frac{1}{2} t_{IJ}^{\alpha} l \tag{22}$$

3.5 Determination of particles associated to element sides

For element sides on coupling interfaces, particles associated to them are required to determine since their stresses are needed for calculating equivalent tractions. Figure 6 shows how these particles are determined. Particle i is associated to element side IJ if the flowing criterion is satisfied

$$\xi_l \leq R_{\mathrm{N}} \leq \xi_h, \quad 0 \leq R_{\mathrm{T}} \leq 1 \tag{23}$$

where $R_{\mathrm{N}} = \delta / r_i$, δ is the penetration distance between particle i and element side IJ, r_i is the radius of particle i which is determined as $r_i = 0.5 h_i / \alpha_h$, $R_{\mathrm{T}} = l_{JO} / l_{JI}$, $l_{JO} = x^{\alpha}_{OJ} x^{\alpha}_{IJ} / \sqrt{x^{\alpha}_{IJ} x^{\alpha}_{IJ}}$, $l_{JI} = x^{\alpha}_{IJ} x^{\alpha}_{IJ} / \sqrt{x^{\alpha}_{IJ} x^{\alpha}_{IJ}}$, $x^{\alpha}_{OJ} = x^{\alpha}_{O} - x^{\alpha}_{J}$, $x^{\alpha}_{IJ} = x^{\alpha}_{I} - x^{\alpha}_{J}$, and ξ_l and ξ_h are specified constants. In Figure 6, point o is the projection of particle i on element side IJ, and the penetration distance δ is defined as

$$\delta = (a x^1_i + b x^2_i + c) - r_i \tag{24}$$

where $a = x^2_J - x^2_I$, $b = x^1_I - x^1_J$ and $c = x^2_I x^1_J - x^1_I x^2_J$. δ is negative when particle i crosses over element side IJ and positive when gap exists between particle i and the element side.

The criterion described by Equation (23) allows some penetration and gap between the element side and its associated particles. The allowed penetration and gap are controlled by constants ξ_l and ξ_h. In our calculation, ξ_l and ξ_h are taken as -1 and 1, respectively. This makes the penetration and gap less than the particle radius.

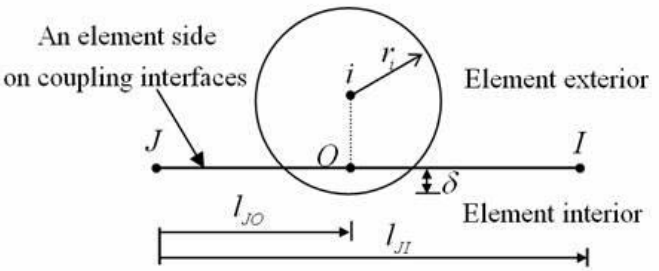

Figure 6: Determination of the association between a particle and an elemental side

The association between particles and element sides is only determined at the beginning of computation. It is considered to be unchanged in the whole computational process. When a particle is associated to an element side, the particle is attached to the element side. It is not allowed to separate from and slide along the element side. To achieve the attachment between particles and element sides, the matching algorithm proposed by Johnson et al. [Johnson, Stryk, Beissel and Holmquist (2002)] is used.

4 Adaptive coupling technique

An adaptive coupling technique is described in this section. For this technique, the initial computational model is entirely composed of elements. During the computational process, severely deformed elements are converted to particles automatically

and the generated particles near coupling interfaces are linked to the elements by the coupling algorithm presented in the previous section. With the adaptive coupling technique, particles can be used as few as possible. Consequently, the computational efficiency of the adaptive coupling will be improved compared with the fixed FEM-SPH coupling, which predetermines the particle regions and element regions.

The adaptive coupling process mainly includes fours steps: (1) Determine distorted elements which should be converted to particles; (2) Determine elements treated as imaginary particles for coupling calculation; (3) Convert element to real particles, and generate imaginary particles; (4) Update the surfaces of element regions and association between particles and element sides. The detailed description for them is given in the following text.

4.1 Determination of elements converted to particles

For triangle element, Minimum Interior Angle (MIA) can effectively reflect the extent of element distortion. Therefore, a MIA criterion is suggested to determine elements which should be converted to particles herein. When the MIA of an element is less than a specified critical value θ_c, the element is considered to be distorted and recorded as one converted to a particle. θ_c is specified as 30° in this paper.

A Group-Based Conversion (GBC) manner is combined with the MIA criterion to determine elements converted to particles. The purpose of this is to simplify the determination of elements treated as imaginary particles and regularize coupling interfaces of element and particle regions. In the GBC manner, elements of each body are divided into groups at the beginning of the computation. During the computational process, if one or more elements in a group satisfy the conversion criterion, then all elements in that group are converted to particles.

Figure 7 illustrates the element grouping for a body meshed with triangular elements. In order to classify the elements into groups a minimum rectangular domain is firstly found to envelop the body. The rectangular domain is then divided into uniform sub-domains with reference size Δ_s, which is determined as

$$\Delta_s = \eta R_{\max} \tag{25}$$

where η is a dilation factor which is the same as that in Equation (8), and $R_{\max}$ denotes the maximum possible radius of influence domains of particles in case all elements are converted to particles. $R_{\max}$ is estimated by

$$R_{\max} = 2h_{\max} = 2\alpha_h \sqrt{A_{0\max}} \tag{26}$$

where $A_{0\max}$ is the maximum initial area of all elements. After determining Δ_s, the

number of sub-domains in x^{α}-direction, $N_{x^{\alpha}}$, can be calculated by

$$N_{x^{\alpha}} = \max\left(Int\left[(x^{\alpha}_{\max} - x^{\alpha}_{\min})/\Delta_s\right], 1\right) \tag{27}$$

and the exact sizes of sub-domains can be given as

$$\Delta x^{\alpha} = (x^{\alpha}_{\max} - x^{\alpha}_{\min})/N_{x^{\alpha}}. \tag{28}$$

The sub-domains are numbered as (I_{x^1}, I_{x^2}) , where I_{x^1} ranging from 1 to N_{x^1} is the index in x^1-direction and I_{x^2} is similar. An element is considered to be in a sub-domain when its gravity center is in the sub-domain. The number of the sub-domain where an element is located can be easily determined by

$$I_{x^{\alpha}} = Int\left[(x^{\alpha}_g - x^{\alpha}_{\min})/\Delta x^{\alpha}\right] + 1 \tag{29}$$

where x^{α}_g are coordinates of the element gravity center. With Equation (29), each element is sorted into a unique sub-domain. Then, all the elements in the same sub-domain compose an element group.

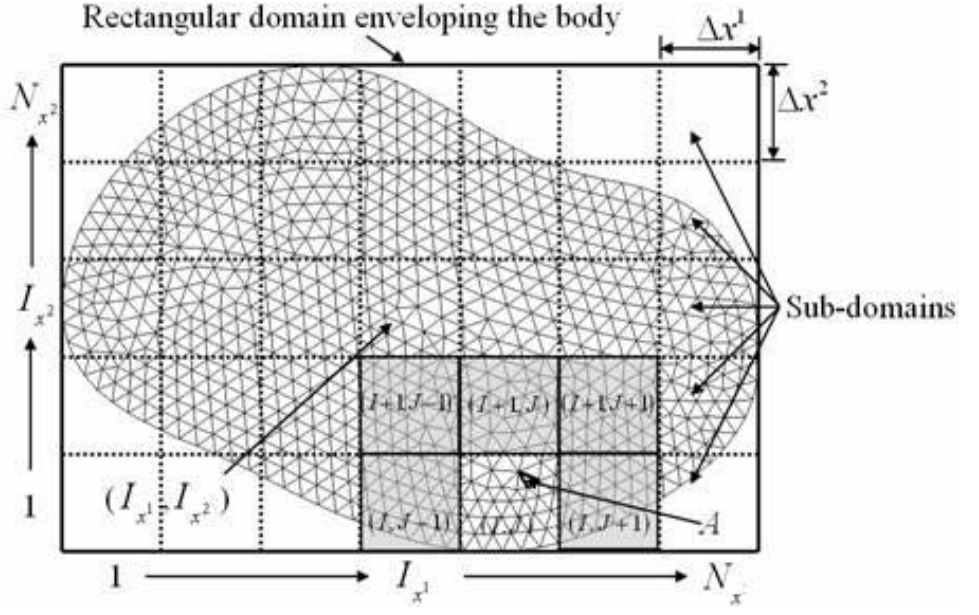

Figure 7: Group-based conversion of elements to particles

4.2 Determination of elements treated as imaginary particles in adaptive coupling

In the adaptive coupling process, the positions of coupling interfaces will change when some elements are converted particles. Thus, elements near coupling interfaces, which are required to treat as imaginary particles for coupling calculation, will also change and should be redetermined. Figure 7 illustrates how to find these elements quickly with the GBC manner. Assuming that element A in group (I,J) satisfies the MIA conversion criterion, all elements in group (I,J) are converted to particles, and all elements in its neighboring groups are treated as imaginary particles. According to the numbering rule in Equation (29), the neighboring groups of group (I,J) are easily obtained as

$$(I\pm 1,J),(I-1,J\pm 1),(I+1,J\pm 1),(I,J\pm 1). \tag{30}$$

There are generally eight neighboring groups for a given group unless it is a boundary group. Among these neighboring groups, some also should be or have been converted particles. In these cases, they are excluded from the groups treated as imaginary particles.

4.3 Conversion of elements to real particles

When an element is converted to a particle, the element is removed from element list and a new real particle is added in particle list. The variables of the new real particle are determined in the same way of imaginary particle which is detailed in section 3.2. Once a real particle is added, its variables are calculated with the SPH equations in the subsequent computation.

4.4 Update of surfaces of element regions and association between particles and element sides

After the conversion of elements to particles, the surfaces of element regions should be updated. Figure 8 shows elements converted to particles at a certain time. The surface of these elements is the loop $N_1-N_2-\cdots-N_{24}-N_1$, which includes line segment $N_1-N_2-\cdots-N_5-N_6$ originally being a part of the surfaces of element regions and line segment $N_6-N_7-\cdots-N_{24}-N_1$ consisting of internal element sides. Once these elements are converted to particles, line segment $N_1-N_2-\cdots-N_5-N_6$ is removed from the surfaces of element regions, and line segment $N_6-N_7-\cdots-N_{24}-N_1$ is added to the surface.

The association between particles and element sides is also necessary to update since coupling interfaces between element and particle regions change when elements are converted to particles. Particles associated to element sides on line

segment $N_6 - N_7 - \cdots - N_{24} - N_1$ are released from them because they are removed. The new particles generated from elements connected to line segment $N_6 - N_7 - \cdots - N_{24} - N_1$ are associated to element sides on the segment.

When the association between the newly generated particles and elements sides is established, there are two typical cases, which are shown in Figure 8. Element A has only one side ($N_6 - N_7$) on the segment. The particle generated from element A is naturally associated and attached to that segment. Element B has two sides ($N_8 - N_9$ and $N_9 - N_{10}$) on the segment. The particle generated from element B is associated to both sides but only attached to the side for which the penetration distance is greater. This treatment follows the idea suggested by Johnson et al. [Johnson, Stryk, Beissel and Holmquist (2002)] for coupling GPA and FEM.

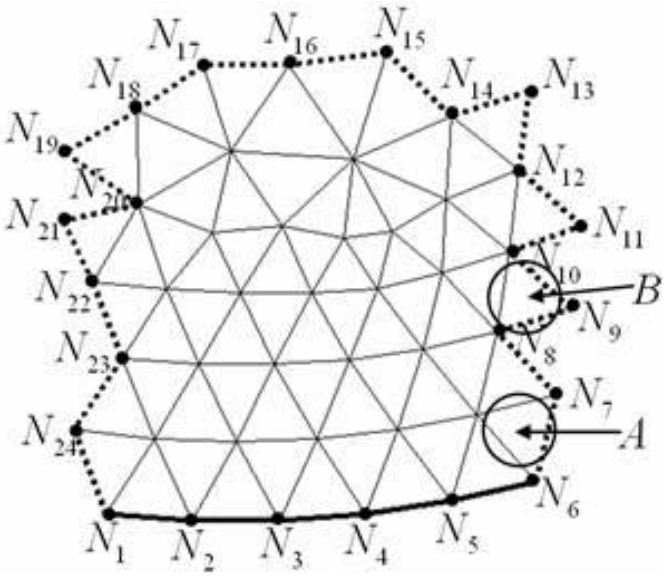

Figure 8: Update of surfaces of element regions after the conversion of elements to particles

5 Numerical examples

In this section, three examples are presented to demonstrate the accuracy and utility of the present coupling algorithm and adaptive coupling technique. The first example is used to test the accuracy of the coupling algorithm through a problem with an analytical solution. The second example is used to test the accuracy of the coupling algorithm and adaptive coupling technique further by comparing with

a commercial code LS-DYNA [Hallquist, 1998]. The third example is presented to show the utility of the adaptive coupling and its advantages compared with the fixed coupling.

5.1 Elastic wave propagation

Figure 9 shows a steel bar impacting a rigid wall with velocity of 50m/s. The bar is assumed to be under plane strain condition and is constrained in the vertical direction. This essentially gives a case of one-dimensional stain in the horizontal direction. Thus, an analytical solution is available for validating numerical solutions.

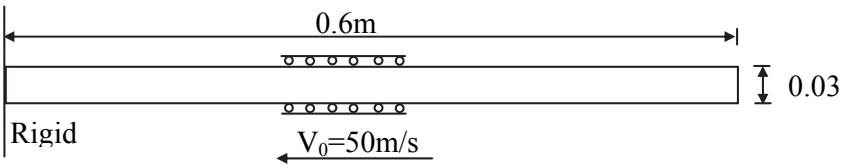

Figure 9: A steel bar impacting a rigid wall

Three coupling algorithms, which are the algorithms in Johnson (1994) and Johnson et al. (2002) as well as the present algorithm, are used to simulate the elastic wave propagation in the impact process. The computational models for the three algorithms are shown in Figure 10(a), (b) and (c), respectively. All models discretize the bar with elements in the left half and particles in the right half. In the present algorithm, the dilation factor η for determining elements treated as imaginary particles is taken as 1.25 since the deformation is slight in this problem. The details of elements treated as imaginary particles, which are marked with dots at element centers, are shown in Figure 10(c).

Figure 11(a) and (b) show the calculated stress distributions at $80\mu s$ by the coupling algorithms in Johnson (1994) and Johnson et al. (2002), respectively. Both algorithms simulate the wave propagation correctly, but stress oscillation is large at the coupling interface ($x = 0.3m$). Figure 11(c) gives the stress result obtained by the present algorithm. The result is in good agreement with the analytical solution and shows nearly no stress oscillation at the coupling interface. Comparing the results of the three algorithms, it is easy to find the present algorithm is more accurate than the other two algorithms. Nevertheless, a little stress jump at the coupling interface is still observed in the result of the present algorithm. This is mainly induced by the difference in the arrangement of real and imaginary particle near the coupling

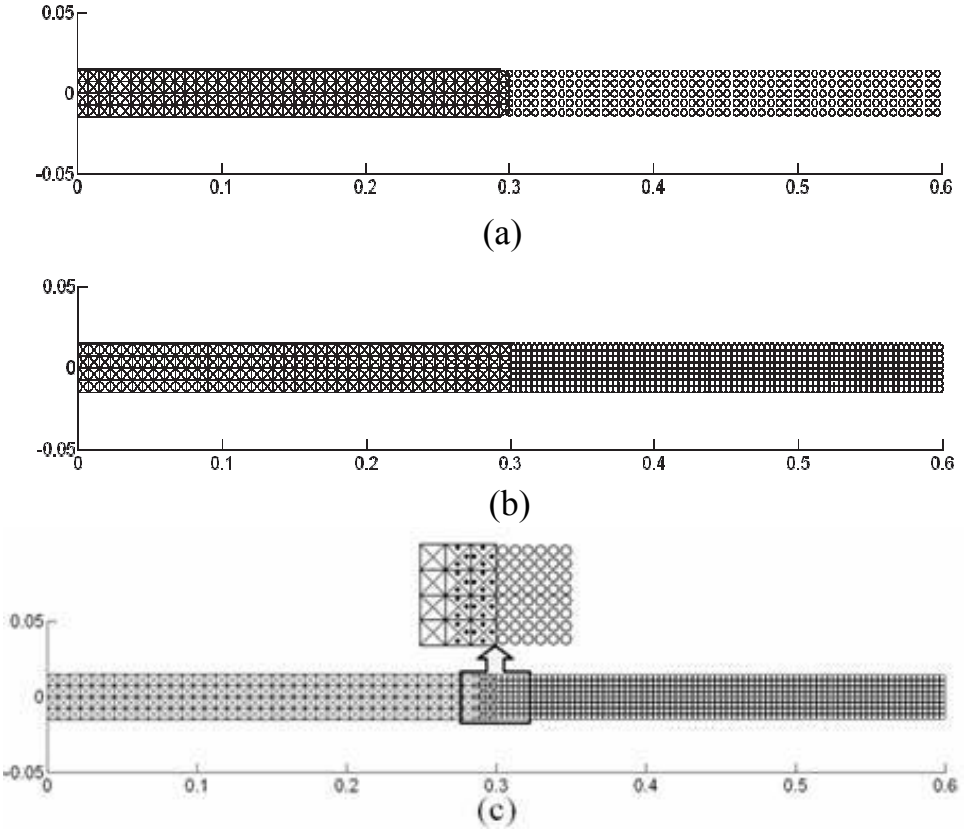

Figure 10: Computational models for three coupling algorithms: (a) algorithm in Johnson (1994); (b) algorithm in Johnson et al. (2002); (c) present algorithm

interface.

Figure 12(a) shows a coupling model where real particle and element arrangements are both crossed. This model provides a completely uniform particle arrangement at the coupling interface since imaginary particle arrangement is also crossed due to the crossed element arrangement. Using crossed particle arrangement, we find the dilation factor α_h for smoothing length should be larger than 1.5 to obtain good stress results even if a pure SPH calculation is performed. Figure 12(b) and (c) shows the calculated stress results of the present algorithm with α_h=1.75 and 2.0, respectively. The calculated stresses show very good agreement with the analytical solution for both two values of α_h, especially for the larger one. No stress jump like that in Figure 11(c) is shown again. This indicates similar particle and

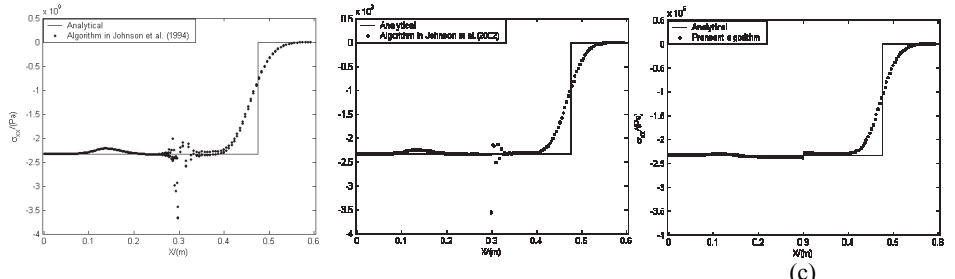

(a) (b) (c)

Figure 11: Stress distributions at $80\mu s$calculated by three coupling algorithms: (a) algorithm in Johnson (1994); (b) algorithm in Johnson et al. (2002); (c) present algorithm

element arrangements at coupling interfaces are preferred to ensure good coupling accuracy for the present algorithm. It is noted that in adaptive coupling particles generated from distorted elements automatically and inherit the arrangement of the replaced elements naturally, so similar particle and element arrangements are usually achieved. From this perspective, the present algorithm is expected to obtain good accuracy for coupling elements and particles in adaptive coupling.

5.2 Elastic-perfectly plastic block impacting a rigid wall

A 7.62mm-width and 25.4mm-height block impacting on a rigid wall with a vertical velocity of 150m/s is simulated in this example. The block material is assumed to be elastic-perfectly plastic. The material properties are taken as density ρ=7850Kg/m^3, Young's modulus E=206GPa, Poisson's Ratio ν=0.3, and yield strength σ_0=1.0GPa.

Fixed and adaptive coupling approaches are used to simulate the problem. The fixed coupling approach predefines the element and particle regions and keeps them unchanged. Figure 13 shows the fixed coupling model, where the bottom quarter of the block is modeled with 1320 particles and the rest is modeled with 4000 elements. The adaptive coupling model completely consists of elements at the initial time. It contains 5280 elements. The finite element algorithm in LS-DYNA is also used to simulate the problem. This provides a reference solution for comparison.

Figure 14 compares the deformed configurations at $40\mu s$ by the fixed and adaptive coupling approaches with that by LS-DYNA. It can be seen the results of the

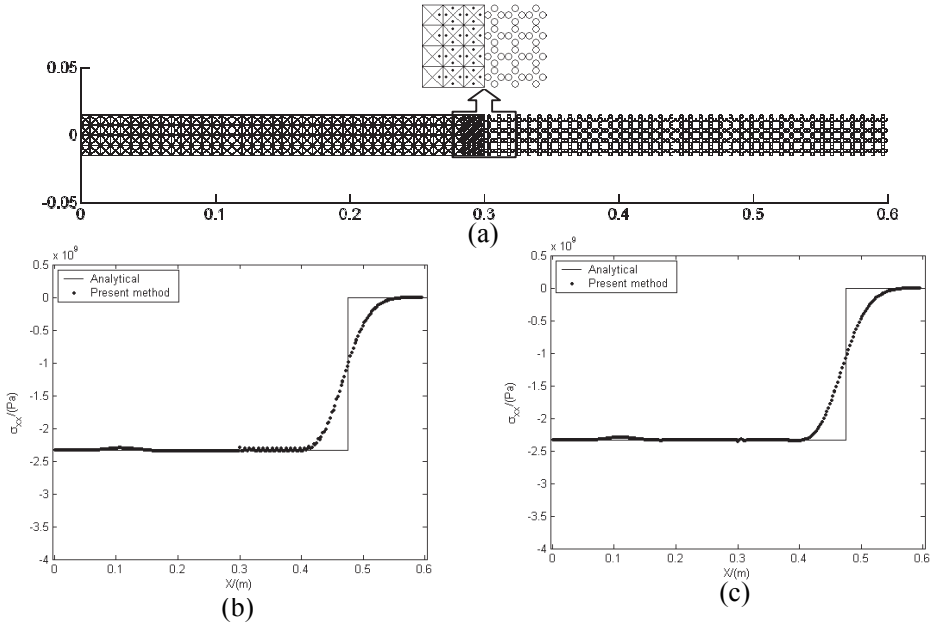

Figure 12: Coupling calculation using model with the same particle and element arrangements: (a) coupling model; (b) result with $\alpha_h = 1.75$; (c) result with $\alpha_h = 2.0$

three approaches are in good agreement. The final heights of the block calculated by LS-DYNA, fixed coupling and adaptive coupling are 23.63mm, 23.67mm and 23.65mm, respectively. The relative error of the height change is 2.4% for the fixed coupling and 1.1% for the adaptive coupling compared with LS-DYNA.

5.3 Oblique impact of a cylinder against a plate

Figure 15 shows a plane strain model of a linear elastic cylinder impacting an aluminum plate. The cylinder is 0.02m in diameter. The plate is 0.4m wide and 0.04m thick. The initial impact velocity is 1000m/s and the angle of incidence is 60°. The cylinder material has a density of 7850Kg/m^3, a Young's modulus of 206GPa, and a Poisson's ratio of 0.3. The plate material is modeled with Johnson-Cook viscoplastic model [Johnson and Cook (1983)]

$$\sigma = (A + B\varepsilon^n)\left(1 + C\ln\frac{\dot{\varepsilon}}{\dot{\varepsilon}_0}\right)\left[1 - \left(\frac{T - T_r}{T_m - T_r}\right)^m\right] \tag{31}$$

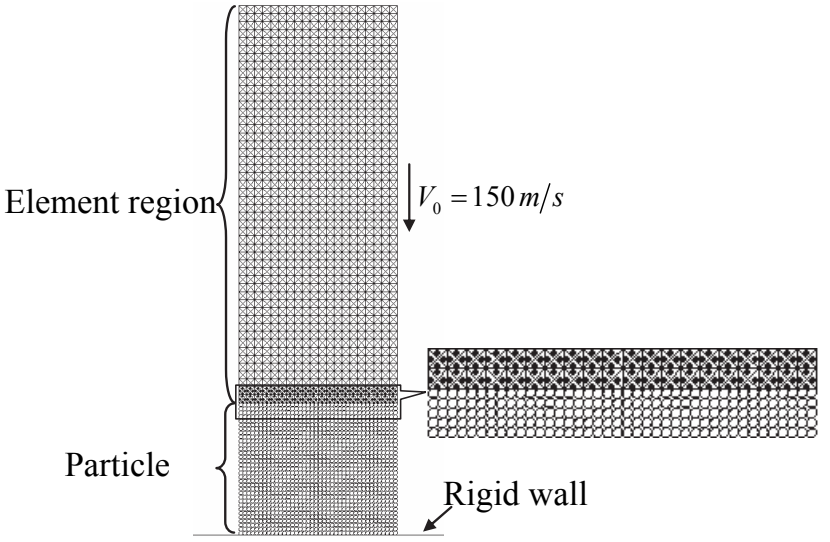

Figure 13: The fixed coupling model for the block impacting a rigid wall

and Mie-Gruneisen equation of state [Libersky, Petschek, Carney, Hipp and Allahdadi (1993)]

$$P(\rho,e) = \left(1 - \frac{1}{2}\Gamma\xi\right) p_H(\rho) + \Gamma\rho e \tag{32}$$

where

$$\xi = \rho/\rho_0 - 1, \tag{33}$$

$$p_H = \begin{cases} a_0\xi + b_0\xi^2 + c_0\xi^3, & \xi \geq 0 \\ a_0\xi, & \xi < 0 \end{cases} \tag{34}$$

and

$$a_0 = \rho_0 C_S^2, \quad b_0 = a_0\left[1 + 2(S_S - 1)\right] \tag{35}$$

$$c_0 = a_0\left[2(S_S - 1) + 3(S_S - 1)^2\right].$$

The properties of the plate material are listed in Table 1. In order to consider the material failure, the tensile pressure is limited to -0.5GPa for the plate material.

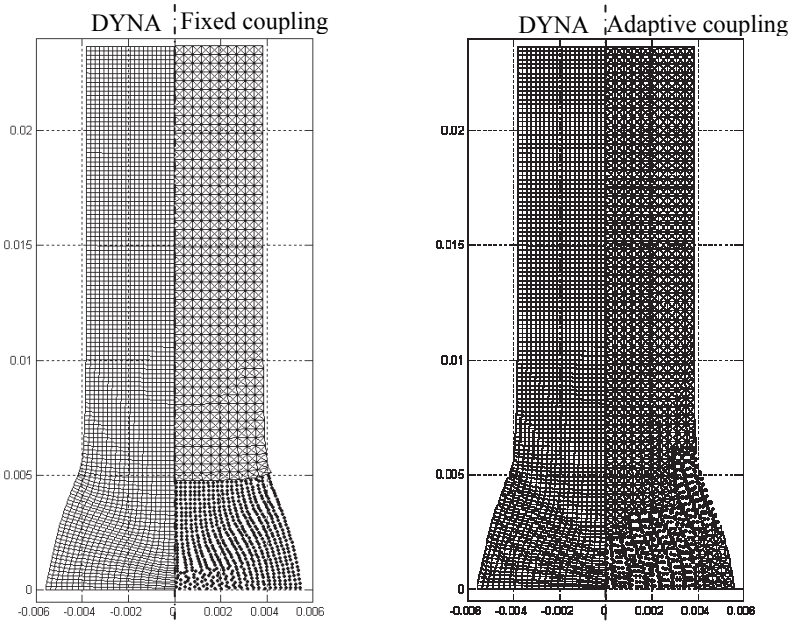

Figure 14: Comparison of the deformed configurations at $40\mu s$

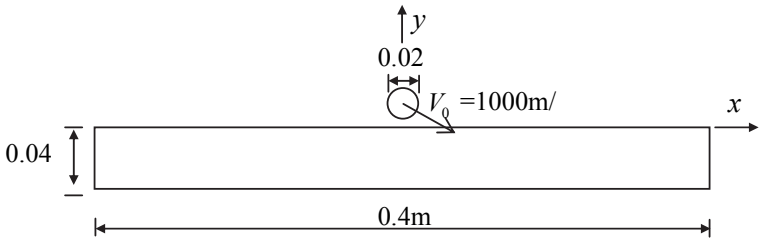

Figure 15: A linear elastic cylinder impacting an aluminum plate

The problem in this example involves extremely large deformations and fractures. The fixed and adaptive coupling approaches are used to simulate the problem. In the fixed coupling model, the cylinder is discretized with 1200 elements since it deforms slight. The plate is wholly discretized with 16000 particles, because it is hard to predict the range of the large deformation and fracture regions. In the adaptive coupling model, the cylinder and plate are initially discretized with 1200

Table 1: The properties of the plate material

ρ (Kg/m^3)	G (GPa)	C_v J/(KgK)	A (GPa)	B (GPa)	n	C	$\dot{\varepsilon}_0$	T_m (K)	T_r (K)	m	C_S (m/s)	S_S	Γ
2710	27.6	875	0.337	0.343	0.41	0.01	1.0	877	300	1.0	5328	1.338	2.0

and 16000 elements, respectively.

Figure 16 shows the deformations of the cylinder and plate at several times calculated with the fixed and adaptive coupling approaches. Figure 17 presents the velocity histories calculated with the two approaches. From these two figures, it can be seen that the results of the two approaches are in good agreement. This implies they achieve equivalent computational accuracy.

With the same computer configuration, the fixed coupling approach costs 143 minutes to complete the simulation, while the adaptive coupling approach costs only 30 minutes. The later is much more efficient than the former. The main reason for this is that little particles are used in the computation of the later. Figure 18 shows the number of real and imaginary particles versus time curves for the adaptive coupling approach. The number of particles increases as the simulation progresses and becomes steady at about $116\mu s$.The final number of particles is only 1972, which is about one eighth of the number of particles in the fixed coupling approach.

6 Conclusions

This paper presents a new coupling algorithm of FEM and SPH as well as an adaptive coupling technique based on the algorithm. Three examples are calculated to demonstrate the accuracy and utility of them. Results of the elastic wave propagation problem shows the present coupling algorithm is accurate and overcomes the stress oscillation in some existing methods. Two different particle arrangements are used to calculate the elastic wave propagation. It is found similar particle and element arrangements at the coupling interface are preferred to ensure good coupling accuracy. For the block impacting a rigid wall, the results of the fixed and adaptive coupling approaches agree well with that of LS-DYNA. This further proofs the validity of the present coupling algorithm and adaptive coupling technique. The calculation of the oblique impact of a cylinder against a plate shows both the fixed and adaptive coupling approaches are capable of modeling extremely large deformations and fractures. We find the two approaches achieve equivalent computational

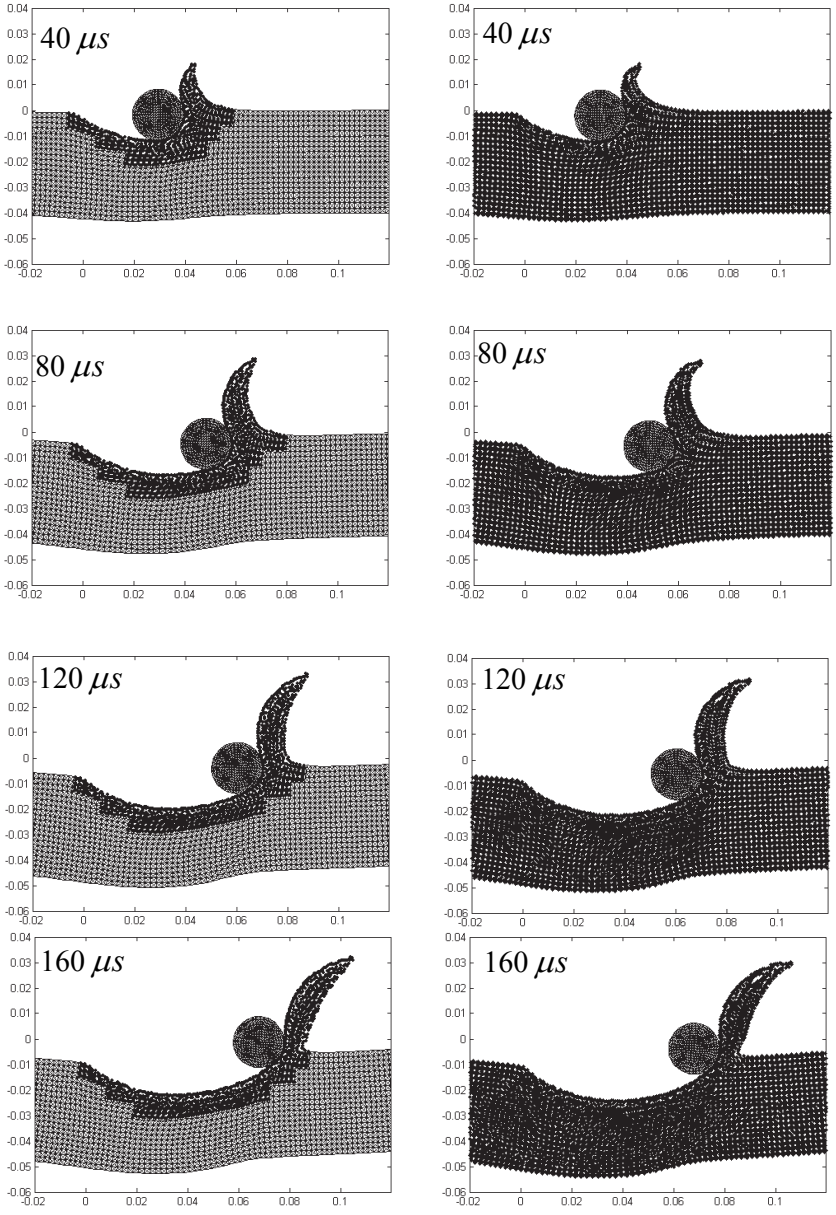

Figure 16: Deformations of the cylinder and plate at several times calculated with the fixed (left) and adaptive (right) coupling approaches

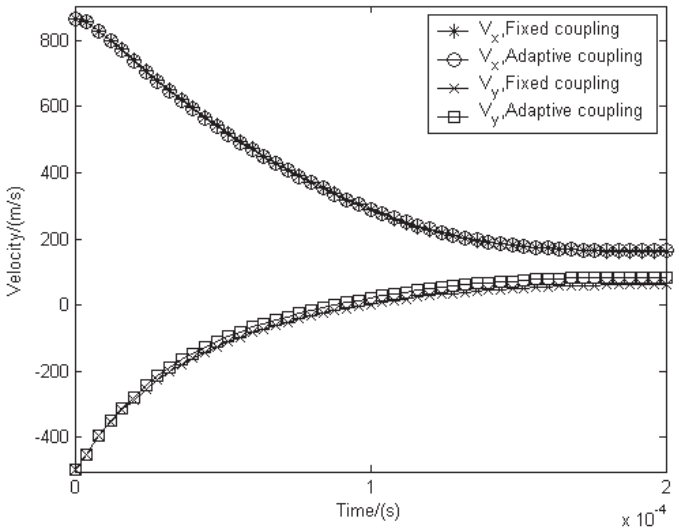

Figure 17: Comparison of the velocity histories calculated with the fixed and adaptive coupling approaches

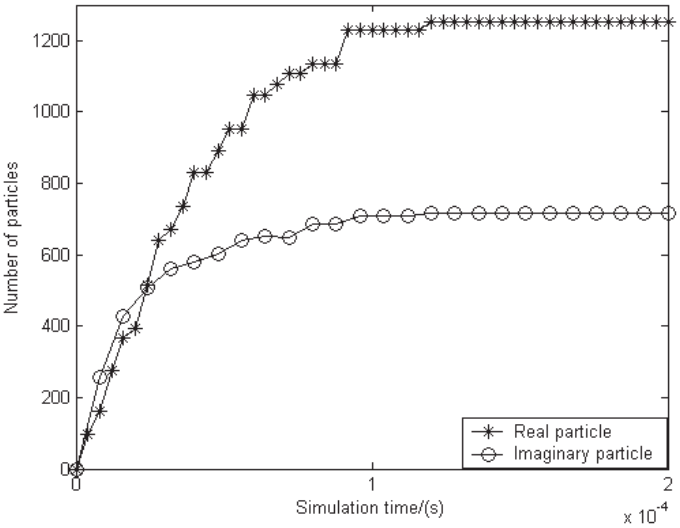

Figure 18: The number of real and imaginary particles versus time curves

accuracy, but the adaptive coupling is much more efficient than the fixed coupling since it can remarkably reduce the particles used in computation.

The present coupling algorithm is simple in implementation. The form of the formulations of FEM and SPH is not needed to change. The extra operations introduced by the coupling are the generation of imaginary particles and the determination of equivalent tractions, which can be easily achieved with the methods presented in the paper. The current coupling algorithm is two dimensional, but it is easy to extend the algorithm to three dimensional problems.

Acknowledgement: The financial support from National Science Foundation of China (10902038) is gratefully acknowledged.

Reference

Attaway, S. W.; Heinstein, M. W.; Swegle, J. W. (1994): Coupling of Smooth particle hydrodynamic with finite element method. *Nuclear Engineering and Design*, Vol. 150, pp. 199-205.

De Vuyst, T.;Vignjevic R.; Campbell, J. C. (2005): Coupling between meshless and finite element methods. *International Journal of Impact Engineering*, Vol. 31, pp. 1054-1064.

Fernández-Méndez, S.; Bonet, J.; Huerta, A. (2005): Continuous blending of SPH with finite elements. *Computers and Structures*, Vol. 83, pp. 1448-1458.

Gray, J. P.; Monaghan, J. J.; Swift, R. P. (2001): SPH elastic dynamics. *Computer methods in applied mechanics and engineering*, Vol. 190, pp. 6641-6662.

Gingold, R. A.; Monaghan J. J. (1977): Smoothed particle hydrodynamics: theory and application to non-spherical stars. *Monthly Notices of the Royal Astronomical Society*, Vol. 181, No. 2, pp. 375-389.

Hallquist, John O. (1998): LS-DYNA theoretical manual. Livermore Software Technology Corporation.

Johnson, G. R.; Cook, W. H. (1983): A constitutive model and data for metals subjected to large strains, high strain rates and high temperatures, Proceedings of the Seventh International Symposium on Ballistics, The Hague, The Netherlands, pp. 541-547.

Johnson, G. R. (1994): Linking of Lagrangian particle methods to standard finite element methods for high velocity impact simulations. *Nuclear Engineering and Design*, Vol. 150, pp. 265-274.

Johnson, G. R.; Stryk, R. A.; Beissel, S. R. (1996a): SPH for high velocity impact computations. *Computer methods in applied mechanics and engineering*, Vol. 139,

pp. 347-373.

Johnson, G. R.; Stryk, S. R.; Beissel, S. R. (1996b): Interface effects for SPH impact computations. Structures under shock and impact IV, pp. 285-294.

Johnson, G. R.; Stryk, R. A.; Beissel, S. R.; Holmquist T. J. (2002): An algorithm to automatically convert distorted finite elements into meshless particles during dynamic deformation. *International Journal of Impact Engineering*, Vol. 27, pp. 997-1013.

Johnson G. R.; Stryk, R. A. (2003): Conversion of 3D distorted elements into meshless particles during dynamics deformation. *International Journal of Impact Engineering*, Vol. 28, pp. 947-966.

Liu, G. R.; Liu, M. B. (2003): Smoothed particle hydrodynamics: A meshfree particle method. World Scientific.

Lucy, L. B. (1977): A numerical approach to the testing of the fission hypothesis. *The Astronomical Journal*, Vol. 82, No. 12, pp. 1013-1024.

Libersky, L. D.; Petschek, A. G.; Carney, T. C.; Hipp, J. R.; Allahdadi, F. A. (1993): High strain Lagrangian hydrodynamics. *Journal of Computational Physics*, Vol. 109, pp. 67-75.

Monaghan, J. J. (1992): Smoothed particle hydrodynamics. *Annual Review of Astronomical and Astrophysics*, Vol. 30, pp. 543-574.

Rabczuk, T.; Xiao, S. P.; Sauer, M. (2006): Coupling of mesh-free method with finite elements: basic concepts and test results. *Communications for Numerical Methods in Engineering*, Vol. 22, pp. 1031-1065.

Sauer, M. (2000): Adaptive Koppling des netzfreien SPH-Verfahrens mit finiten Element zur Berechnung von Impakvorgaengen. Dissertation, Universitaet der Bundeswehr Muenchen, Institut fuer Mechanic und Statik.

Sauer, M.; Hiermeier, S.; Scheffer, U. (2001): Modeling penetration events using FE/MLSPH adaptive coupling. 10th International Symposium on Interaction of the Effect of Munitions with Structures, San Diego, California, U.S.A, May 7-11.